Organosilane Self-Assembled Monolayer Growth from Supercritical Carbon Dioxide in Microstructured Optical Fiber Capillary Arrays

ARTICLE *in* LANGMUIR · MAY 2008

Impact Factor: 4.46 · DOI: 10.1021/la703155z · Source: PubMed

5 AUTHORS, INCLUDING:

Mehmet Fatih Danisman
Middle East Technical University
17 PUBLICATIONS **596** CITATIONS
SEE PROFILE

David L Allara
Pennsylvania State University
259 PUBLICATIONS **22,890** CITATIONS
SEE PROFILE

John V Badding
Pennsylvania State University
187 PUBLICATIONS **2,542** CITATIONS
SEE PROFILE

Organosilane Self-Assembled Monolayer Growth from Supercritical Carbon Dioxide in Microstructured Optical Fiber Capillary Arrays

Mehmet F. Danışman,[†,‡] Jacob A. Calkins,[†] Pier J. A. Sazio,[§] David L. Allara,*[,†] and John V. Badding*[,†]

Department of Chemistry, Pennsylvania State University, University Park, Pennsylvania 16802, and Optoelectronics Research Centre, University of Southampton, Southampton, S0171BJ, UK

Received October 11, 2007. In Final Form: December 6, 2007

Microstructured optical fibers form a new class of extreme aspect ratio templates that are well-suited for precise, designed spatial organization of materials and molecules at dimensions down to the nanoscale. The extreme aspect ratios of the nanoscale to microscale pores in the templates necessitates new approaches to fabrication of nanowires, nanotubes, and self-assembled monolayers within them. High-pressure fluids, which have lower viscosities than liquids and no surface tension, are well-suited for penetrating such extreme aspect ratio capillaries. Here we report an approach to fabricating self-assembled monolayers within microstructured optical fibers using near supercritical or supercritical carbon dioxide. An AFM-based "shaving" technique has been developed to characterize the monolayers formed in capillaries that are too small to allow for characterization by conventional approaches.

1. Introduction

Organizing matter with great precision at dimensions down to the nanoscale is essential to the fabrication of advanced materials and devices. Microstructured optical fibers are a new class of template that can have pores of less than 10 nm dimensions organized into arrays with specific and precisely designed periodic or aperiodic geometries.[1,2] The geometry of the pores can be designed to flexibly control the propagation of waveguided light (e.g., dispersion, modal properties, photonic bandgaps) within the fibers. Embedding materials within the fiber templates provides a powerful and flexible means to both spatially organize them and allow for interaction over very long length scales with waveguided light in the fiber core or matter flowing down the capillary holes. These interactions can be exploited for a broad range of applications, such as chemical and biological sensing and optoelectronic modulation, detection, and generation of light. It has been recently shown that solid-state materials such as semiconductors and metals can be integrated into the arrays of pores of the microstructured optical fibers over lengths of nearly 1 m via deposition from flowing high-pressure fluids.[2] Annular layers of materials such as silicon and germanium can be deposited within micro- to nanoscale holes until the central hole from which deposition occurs is less than 10 nm in diameter, illustrating the ability of flowing high-pressure fluids to overcome the severe mass transport constraints imposed by extreme aspect ratio submicron diameter capillaries.[2] Arrays of semiconductor microwires and nanowires precisely spatially organized in virtually any desired geometry can be made by this approach. Surface chemistry plays a critical role in these deposition processes, especially in view of the increasing surface area to volume ratio as the capillary diameter decreases to nanoscale dimensions.

Here we report the formation of alkylsiloxane self-assembled monolayers (SAMs) within microstructured optical fibers from precursors dissolved in flowing high-pressure media. Molecules and polymers are of increasing interest for photonics and can exhibit exceptional nonlinear and electro-optic properties for applications such as frequency conversion using third-order nonlinearities, optical modulators based on Mach−Zender interferometers, lasers based on molecular gain media, and optical isolators that exploit the capabilities of molecules to rotate light.[3] Fiber technology is dominant in telecommunications and is of increasing interest in many other application areas, such as chemical sensing. Incorporating frequency conversion, optical gain, and modulation capabilities directly into active fiber devices, without having the light exit the fiber, is thus of considerable technological interest.[2] For such applications, the molecules must be integrated into fibers in the form of layers with high geometric perfection over distances of 1 m or more in pores with dimensions down to the nanoscale. The waveguided light in the fiber can then interact with these molecular layers to enable the aforementioned applications. The fiber pores fabricated during the drawing process are nearly atomically smooth, having a root-mean-square roughness of ∼0.1 nm; even slight increases in this value will result in undesirable increases in optical loss for waveguided light.[4] SAMs deposited within the fiber pores should have the required geometric perfection; additional molecular layers can be strategically deposited upon the SAMs to assemble thicker films that will exhibit stronger interaction with the light. Other applications for integrated SAMs can be envisioned in areas such as microfluidics and nanofluidics, chemical separations, and chemical sensing. The surface hydrophobicity is of central importance to flow in nanoscale pores, and this work provides a means to functionalize such pores for nanofluidic applications.

Similar to the cases of deposition of semiconductor and other solid-state materials in silica fiber pores, molecular deposition will require conditions such as *flowing* high-pressure fluids in order to overcome critical issues associated with mass transport

* Corresponding authors. E-mail: dla3@psu.edu (D.L.A.), jbadding@chem.psu.edu (J.V.B.).

† Pennsylvania State University.

‡ Current address: Department of Chemistry, Middle East Technical University, TR-06531 Ankara, Turkey.

§ University of Southampton.

(1) Knight, J. C. *Nature* **2003**, *424*, 847.

(2) Sazio, P. J. A.; Amezcua-Correa, A.; Finlayson, C. E.; Hayes, J. R.; Scheidemantel, T. J.; Baril, N. F.; Jackson, B. R.; Won, D. J.; Zhang, F.; Margine, E. R.; Gopalan, V.; Crespi, V. H.; Badding, J. V. *Science* **2006**, *311*, 1583.

(3) Ma, H.; Jen, A. K. Y.; Dalton, L. R. *Adv. Mater.* **2002**, *14*, 1339.

(4) Roberts, P. J.; Couny, F.; Sabert, H.; Mangan, B. J.; Williams, D. P.; Farr, L.; Mason, M. W.; Tomlinson, A.; Birks, T. A.; Knight, J. C.; Russell, P. S. J. *Opt. Express* **2005**, *13*, 2364.

10.1021/la703155z CCC: $40.75
Published on Web 02/27/2008

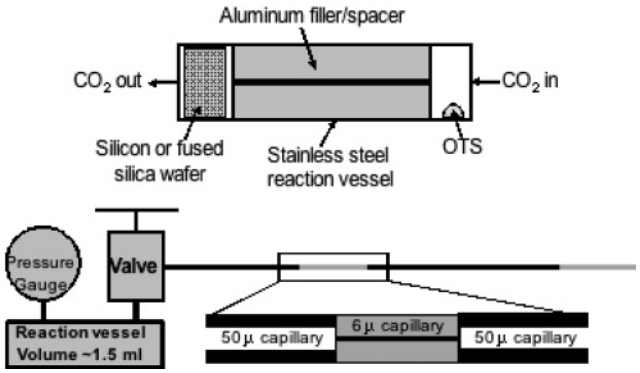

Figure 1. Schematic of the reaction vessels used for OTS deposition on wafers (top panel) and in capillaries (bottom panel).

arising from the extreme aspect ratio containment. There is an extensive literature reporting functionalization of capillaries of approximately 50 μm diameter or larger via solvent-based approaches and the characterization of the deposited films by measurements of electroosmotic flow characteristics and durability.[5,6] However, in approaching the much smaller diameters in nanostructured optical fibers, it is not clear that these methods will provide the necessary quality and performance of the films, e.g., highly uniform coverages with high conformality to the pore walls, and new methods must be carefully validated as each diminishing diameter scale is reached. In addition, the surface tension of liquid water has been found to destroy "large air fraction honeycomb" microstructured optical fibers with delicate silica pore walls only ~30 nm thick (an example of such a honeycomb fiber is shown in Figure 1e of ref 2). On the basis of previous work, a good starting point would appear to be the use of high-pressure, low-surface-tension fluids, in particular supercritical fluids with vanishing interfacial tension. Carbon dioxide, near ($ncCO_2$) or at the supercritical point ($scCO_2$), for example, has a viscosity approximately 1 order of magnitude less than that of a typical liquid and, when driven by a substantial pressure drop, can readily penetrate even nanoscale pores.

In these first experiments, we chose $scCO_2$ as the deposition medium for the formation of octadecylsiloxane SAMs in our porous optical fibers. Deposition of similar monolayers on planar SiO_2, mesoporous silica, and metal oxide surfaces from $scCO_2$ has been reported,[7−11] and we used this as a starting point with octadecyltrichlorsilane (OTS) as the precursor. The OTS SAMs were formed within capillary pores of diameters as small as 6 μm with aspect ratios as large as 5×10^4. The central challenge in this work was to accurately characterize the SAMS in terms of the coverage and uniformity in these small, curved structures. In previous studies in which microchannel or capillary walls were coated with silanes in order to alter the electro-osmotic flow and/or wetting characteristics and fluid dynamics, film density and quality were not characterized thoroughly. As a result, likely due to the variations in the film coverage, substantial variations in the results of different groups that employ similar techniques were reported.[5,12,13] In addition, this lack of knowledge of film coverage prevents an independent study of the coverage and wettability inside the channels.[12] In order to minimize such ambiguities, we employed contact angle measurements as a measure of film coverage and organization and developed a novel AFM-based "shaving" technique to evaluate film thickness. We find that while liquid solvents could have been used to functionalize the interior surface of the large capillaries, such as those near or larger than 50 μm diameters, this method does not appear to work for significantly smaller diameters and long fiber lengths approaching meters. In contrast, the $scCO_2$ method appears highly tractable to nanoscale dimensions. Attempts were also made to characterize the SAMs using microreflectance infrared and microRaman spectroscopies, but signal/noise limitations appear to limit the use of these techniques for monolayers.

Initially, we investigated deposition from high-pressure CO_2, but this involved processing steps including liquid water and liquid chloroform, which would preclude silanization of microstructured optical fibers with capillaries of nanoscale dimensions with extreme aspect ratios. Thus, we also investigated using water and chloroform dissolved in high-pressure CO_2 for the introduction of surface hydroxyl groups on the pore walls and flushing away of excess OTS, respectively, an approach that works as well as the one involving liquid water and chloroform.

2. Experimental Section

2.1. Materials. OTS (99% purity; Sigma-Aldrich) was used as received from containers freshly opened in an inert atmosphere box. Hexadecane (Sigma-Aldrich, 99$^+$% anhydrous) was used as received. Water was purified to remove organic and ion impurities (Milli-Q grade water; Millipore Products, Bedford, MA). Silicon wafers (2 in., n-doped with one side polished to ~0.2 nm rms roughness) and fused silica slides (~0.8 nm rms roughness) were used as substrates. One side of the fused silica slides was roughened by grit blasting in order to minimize interference effects during the IR-reflection measurements. Silica capillaries and microstructured optical fibers of various diameters (~0.1 nm rms roughness) were prepared using the University of Southampton Optoelectronics Research Centre's fiber-drawing facilities.

2.2. Cleaning of Silicon Wafers, Fused Silica Slides, and Microstructured Optical Fiber Capillaries. Silicon wafers were first ultrasonically degreased in chloroform for 5 min followed by 5 min of immersion in a concentrated H_2SO_4/H_2O_2 (30%) 3:1 (v:v) mixture (Piranha solution) at 80 °C (**Caution:** *reacts violently with organics*) and thoroughly rinsed with purified water. After a final rinsing with ethanol, the substrates were dried in a nitrogen stream and then cleaned by UV/ozone exposure for 15 min. After a second cycle of cleaning, reference ellipsometric and reflection absorption IR measurements were immediately made. Following these measurements, a final UV/ozone treatment was performed, and the substrates were kept in purified water overnight until silanization. The fused silica slides were treated the same way as the silicon wafers, except that the samples were immersed in boiling water for several hours. Silica capillaries and microstructured optical fibers were used as received after drawing without any cleaning steps. Just prior to silanization, however, unless otherwise specified, they were flushed with purified water (either room temperature or boiling) overnight to increase the surface concentration of hydroxyl groups. For experiments that employed principally $ncCO_2$, the microstructured optical fibers were flushed with wet CO_2 at 25 °C for 48 h, followed by a 2 h nitrogen flush. The wet CO_2 was prepared by dissolving 100 μL of purified water in 3 mL of CO_2 at 34.4 MPa and 100 °C; preparation was done above room temperature to facilitate dissolution. As drawn, the capillary interiors are expected to have a very low surface concentration of hydroxyl groups.

(5) Doherty, E. A. S.; Meagher, R. J.; Albarghouthi, M. N.; Barron, A. E. *Electrophoresis* **2003**, *24*, 34.
(6) Belder, D.; Ludwig, M. *Electrophoresis* **2003**, *24*, 3595.
(7) Combes, J. R.; White, L. D.; Tripp, C. P. *Langmuir* **1999**, *15*, 7870.
(8) Shin, Y.; Zemanian, T. S.; Fryxell, G. E.; Wang, L. Q.; Liu, J. *Microporous Mesoporous Mater.* **2000**, *37*, 49.
(9) Cao, C. T.; Fadeev, A. Y.; McCarthy, T. *Langmuir* **2001**, *17*, 757.
(10) Zemanian, T. S.; Fryxell, G. E.; Liu, J.; Mattigod, S.; Franz, J. A.; Nie, Z. M. *Langmuir* **2001**, *17*, 8172.
(11) McCool, B.; Tripp, C. P. *J. Phys. Chem. B* **2005**, *109*, 8914.
(12) Neto, C.; Evans, D. R.; Bonaccurso, E.; Butt, H. J.; Craig, V. S. J. *Rep. Prog. Phys.* **2005**, *68*, 2859.
(13) Munro, N. J.; Huhmer, A. F. R.; Landers, J. P. *Anal. Chem.* **2001**, *73*, 1784.
(14) Hoffman, R. L. *J. Colloid Interface Sci.* **1975**, *50*, 228.

2.3. Silanization of Silicon Wafers and Fused Silica Slides. Silanization of silicon and silica substrates was carried out in a stainless steel high-pressure vessel having a volume of ~30 mL (Figure 1). The vessel was loaded into an inert atmosphere, humidity-free glove box. The substrates were placed in one end of the vessel and a nominal 50 μL aliquot of OTS was placed at the other end. The vessel was sealed, immediately connected to a gas delivery line, and pressurized to 10.3 MPa with pure CO_2 by means of a Newport Scientific 207 MPa dual-stage pump. As the pressure increases, the OTS is forced to flow through a 1 mm wide channel into the opposite end of the vessel containing the substrates. Once the CO_2 solvent density becomes high enough, the OTS dissolves in the CO_2 fluid. After letting the reaction proceed for a desired period, the vessel was vented and then purged several times with CO_2. Finally, the wafers were removed and ultrasonically cleaned in chloroform for at least 5 min.

2.4. Silanization of Silica Capillaries and Microstructured Optical Fibers. For silanization of the silica microstructured optical fiber capillaries, first a desired amount of OTS was placed in the high-pressure vessel in the glove box (Figure 1). After CO_2 pressurization, the silica capillaries were attached via a high-pressure fitting with a valve at the vessel. The valve was opened to allow the CO_2/OTS mixture to flow through the capillaries. When large diameter (50 μm) capillaries were used, small diameter (6 μm) capillaries were spliced to the end the of the larger diameter ones in order to limit the flow rate. After a desired period of time, the capillaries were detached from the vessel and flushed with pure CO_2 for approximately 1 h. The OTS-coated capillaries then were immersed in an ultrasonic bath filled with water while chloroform was drawn through the capillaries. This treatment was followed by CO_2 and N_2 gas purges. For experiments that employed principally $ncCO_2$, the microstructured optical fibers were flushed for 12 h at room temperature with 150 μL of chloroform dissolved in 3 mL of $ncCO_2$ (prepared at 29.6 MPa at 60 °C for 1 h; preparation was done above room temperature to facilitate dissolution) instead of sonicating in liquid chloroform.

2.5. Single-Wavelength Ellipsometry (SWE) Measurements. A Stokes ellipsometer (Gaertner Scientific Corp., Skokie, IL) was used with a 632.8 nm beam set at an incidence angle of 70°. The film thicknesses were determined by employing an isotropic air/SAM/substrate model, with the real and imaginary parts of the film refractive index set to 1.5 and 0, respectively. The bare substrate was measured and this value converted to a reference psuedo-optical function for the film thickness calculations. Since the refractive indices of the organic film and pure silica are so close, the film thicknesses could only be determined for the silicon substrates.

2.6. Contact Angle Measurements. Hexadecane contact angles were measured on the silicon wafers and silica slides with a home-built sessile drop instrument. First, a droplet of the probe liquid was dispensed on the surface, by means of a flat-tipped micrometer syringe. The image of the drop was then captured digitally, while the drop was being expanded (contracted) for determining the advancing (receding) angle. Alternatively, the advancing and the receding angles were determined by pulling the drop on the surface at a constant speed by means of a micromanipulator. The images captured either way were then analyzed by using image analysis software (ImageJ, National Institutes of Health).

2.7. Capillary Contact Angle Measurements. Water "contact angles" inside the silica capillaries were measured at an air/liquid interface of a column of water (or a bubble of air in between two columns of water) inside the capillaries (Figure 2). A slight pressure was applied to the liquid reservoir to force the water to move, and the meniscus position was monitored with an optical microscope. The average meniscus speed was set in a range between ~0.1 and 10 μm/s, for which the dependence of the meniscus shape on speed was effectively constant. The image from the microscope was captured digitally and the air/water interface angle at the capillary wall determined. We note that the "raw" contact angles for the capillary geometries ideally need to be corrected for optical refraction effects and variations in imaging parameters such as lighting and focusing. These corrections can be made to some extent by considering the full curvature of the water meniscus. Since, this latter method is also not free of errors and since we were only interested in the relative change in the contact angles with surface treatment, we just report the raw contact angles. (For the correlation between the raw and "apparent" contact angles, extracted from the curvature of meniscus, and a detailed explanation of the errors, see ref 14.)

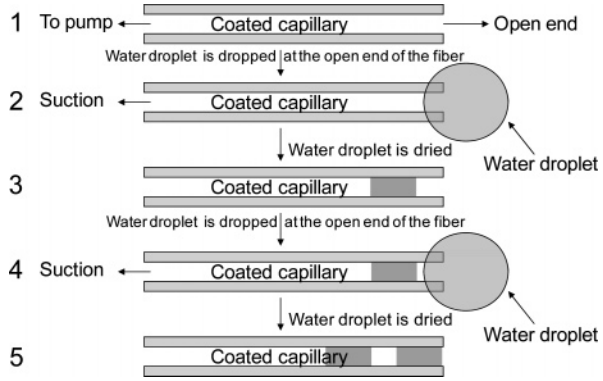

Figure 2. Schematic representation of the procedure employed for contact angle measurements in capillaries.

2.8. Atomic Force Microscopy on Planar Surfaces and Capillary Interiors. A Dimension 3100 scanning probe microscope (Digital Instruments, Santa Barbara, CA) was used for atomic force microscopic imaging. For tapping-mode imaging of n-doped Si, tips with radii of 10 nm and force constants of 50 N/m were used (Veeco, Santa Barbara, CA). For contact-mode imaging and indentation experiments, similar tips but with force constants of 3 N/m were used (Nanosensors, Neuchatel, Switzerland).

For imaging the films inside the capillaries, short sections of the capillaries were placed on double-sided tape and crushed. Next, the pieces presenting the inner walls of the capillaries upward were identified by the AFM's optical microscope and then imaged in the selected mode. AdvancedTEC tips (Nanosensors, Neuchatel, Switzerland) were used since these tips extend further away from the cantilever than the standard tips and are more clearly visible.

Nanoindentation experiments were carried out as follows: The films were first imaged by contact mode imaging at low force (50 nN). Small regions at the center of the previously imaged areas then were scanned at high force (1000−2000 nN) to remove (shave) film material and the regions again imaged at low force to image the shaved areas. The average indentation depths of the shaved regions were determined by using the "stepheight" tool of the NanoScope software (v5.12r5, Digital Instruments, Santa Barbara, CA).

2.9. Reflection IR Spectroscopy Measurements. An in-house-modified Fourier transform spectrometer (Bio-Rad FTS-7000/Digilab, Randolph, MA) with external sample−detector optics housed in a N_2 or dry air (H_2O and CO_2 free) purge box was used. For fused silica substrates s-polarized light with an 80° incidence angle was used. For the doped silicon substrates p-polarized light at 86° was used. Spectra were recorded at 4 cm^{-1} resolution and 1600 scans were coadded in order to improve the signal-to-noise ratio. Spectral intensities are reported as $-[\log(I/I_0)]$, where I and I_0 are the reflection intensities from the sample and the reference surfaces, respectively. Freshly cleaned bare silicon and fused silica surfaces were used as references, as detailed in the sample preparation section.

3. Results and Discussion

3.1. Film Formation on Planar Substrates. We first investigated OTS film formation on the planar substrates, since more characterization tools are suitable for these samples than for the capillaries. The information obtained from the planar surfaces thus provided a general understanding of the factors that affect film growth and structure and served as a starting

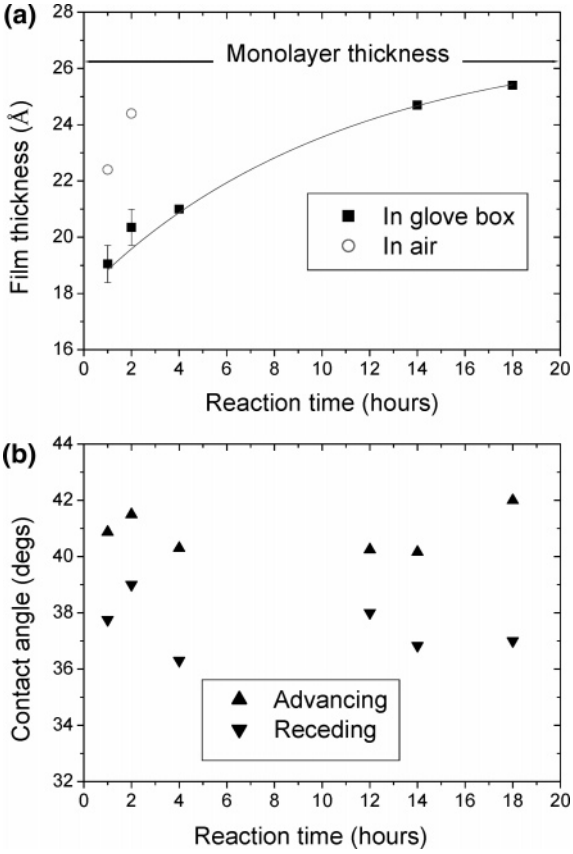

Figure 3. Ellipsometric thickness (a) and (hexadecane) contact angles (b) of OTS films on native oxide silicon surfaces as a function of reaction time. The solid line in part a is a guide to the eye.

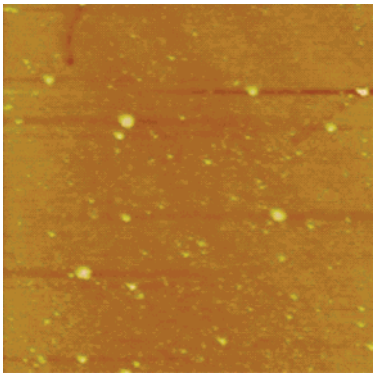

Figure 4. Tapping-mode AFM image of a high-coverage OTS film on a native oxide silicon surface. Image size = 5 × 5 μm^2, *z*-scale = 10 nm.

point for optimized growth conditions in the highly curved and confined geometries of the fiber pores.

3.1.1. Ellipsometry, Wetting, and Infrared Spectroscopy. Ellipsometrically deduced thicknesses of the films grown on silicon wafers as a function of reaction time are shown in Figure 3a. Almost 80% of the film coverage occurs in the first few hours. After ~18 h, the coverage approaches the ideal limiting thickness of ~26 Å for vertical chains.[24] When the OTS concentration in the reaction vessel was increased (by using 100 μL and 1 mL OTS, instead of 50 μL), after 18 h of reaction, observed film coverages exceed the limiting monolayer value (data not shown). For these latter high coverage films, polymerized OTS clusters were observed by AFM (Figure 4) on otherwise smooth monolayers of OTS. We also studied the effect of the humidity level in the reaction vessel by sealing the reaction vessel in air, instead of the glove box. As can be seen in Figure 3a film growth was much faster in the presence of air.

These results, which are in agreement with previous CO_2 studies,[7,9] indicate that OTS film growth on native oxide SiO_2 in either $scCO_2$ or $ncCO_2$[31] follows a similar mechanism to that in conventional organic solvents. In the organic solvents, a fast initial formation of densely packed regions on the water-rich areas at the surface is followed by a slower growth step, during which the film density increases slowly on the water-poor regions and the insertion of the free OTS molecules in the already dense regions takes place.[15−20] As a result, though the majority of the adsorption occurs early during the film growth, regardless of the water concentration on the surface, the coverage attains its maximum value in a much shorter time when the surface water content is high. However, here we note that, while in the case of the organic solvents, the hydrolysis of the chlorosilane molecules takes place mostly on the surface, when $scCO_2$ is used as the solvent, hydrolysis is expected to occur primarily in the solvent, since the surface water is heavily extracted by $scCO_2$.[7,21] Since the surface water content is not only important for the hydrolysis of the silane molecules but also for the diffusion of the adsorbates on the surface, in $scCO_2$ one might expect more limited surface diffusion and thus a less organized film morphology. In fact, all the advancing (hexadecane) contact angles are higher than 40° with a maximum value of 42° ± 2° (Figure 3b), an indication of a reasonably densely packed film. Though this value approaches the advancing angles reported for a highly organized monolayer of OTS,[22] nominally in the range of 43°−46°, the well-organized films show no measureable hysteresis between the advancing and receding angles,[23,24] while for our films the values vary over 2°−5°. These results indicate the existence of defects on the surfaces that we ascribe to the effects of lower surface hydration in the $ncCO_2$ deposition compared to standard hydrocarbon or low-polarity solvents.

Finally, to determine the alkyl chain configurations in the films, we recorded IR reflection spectra of a film with an ellipsometric thickness of 24.7 Å and hexadecane advancing and receding angles of 40° and 37°, respectively. As can be seen in Figure 5, the peaks due to C−H symmetric (d^+) and antisymmetric (d^-) stretching modes appear at 2849 and 2917 cm^{-1}, respectively. These results indicate that the alkyl chains are highly extended with dominantly trans conformations.

Since growth of dense OTS films depends strongly on surface silanol groups and since fused silica surfaces in ambient environments typically exhibit lower coverages of surface silanol groups than the native oxide surfaces, we designed specific pretreatment procedures to increase the surface silanol coverages on the fused silica surfaces. Since the microcapillaries are formed as pristine silica from melt drawing, conditions developed for film formation on the planar fused silica surfaces were used as the starting point for conditions in the capillary samples. In general, as expected, for the fused silica surfaces, the pretreatment procedures were observed to be more critical than for the native

(15) Darr, J. A.; Poliakoff, M. *Chem. Rev.* **1999**, *99*, 495.
(16) Iimura, K.; Nakajima, Y.; Kato, T. *Thin Solid Films* **2000**, *379*, 230.
(17) Liu, Y.; Wolf, L. K.; Messmer, M. C. *Langmuir* **2001**, *17* (14), 4329.
(18) Bierbaum, K.; Grunze, M.; Baski, A. A.; Chi, L. F.; Schrepp, W.; Fuchs, H. *Langmuir* **1995**, *11*, 2143.
(19) Carraro, C.; Yauw, O. W.; Sung, M. M.; Maboudian, R. *J. Phys. Chem. B* **1998**, *102*, 4441.
(20) Vallant, T.; Brunner, H.; Mayer, U.; Hoffmann, H.; Leitner, T.; Resch, R.; Friedbacher, G. *J. Phys. Chem. B* **1998**, *102*, 7190.
(21) Tripp, C. P.; Combes, J. R. *Langmuir* **1998**, *14*, 7350.
(22) Parikh, A. N.; Liedberg, B.; Atre, S. V.; Ho, M.; Allara, D. L. *J. Phys. Chem.* **1995**, *99*, 9996.
(23) Brzoska, J. B.; Benazouz, I.; Rondelez, F. *Langmuir* **1994**, *10*, 4367.
(24) Parikh, A. N.; Allara, D. L.; Azouz, I. B.; Rondelez, F. *J. Phys. Chem.* **1994**, *98* (31), 7577.

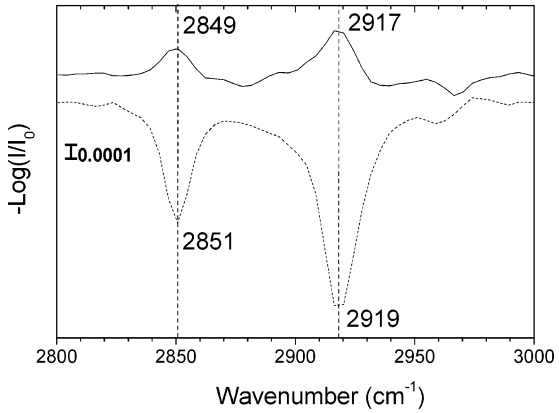

Figure 5. IR reflection spectra of OTS films on native oxide silicon (solid line) and fused silica surfaces (dashed line).

oxide. When the fused silica substrates were treated with water soaks at room temperature or elevated temperatures below boiling, the advancing hexadecane contact angles for the resulting films were always less than 40°, even when a high concentration of OTS was used and/or atmospheric humidity was allowed in the reaction vessel. Only when the substrate was kept in boiling water for several hours before silanization was a high coverage film obtained. With this pretreatment, hexadecane advancing and receding angles of 41° and 36° were observed, respectively. The IR reflection spectrum of the same film (Figure 5) shows that d^+ and d^- peaks appear at 2851 and 2919 cm^{-1}, respectively, which indicates the presence of well-organized chains but with slightly less dense packing and chain conformational ordering than for the native oxide substrate based films.

3.1.2. Atomic Force Microscopy. Because neither SWE nor IR are directly applicable in microcapillaries, we focused on extending the AFM characterization. Of primary importance was the use of AFM "shaving" as a measure of film thickness, in the light of previously reported nanoindentation studies.[25−28] As a preliminary investigation, films having different OTS coverage on planar fused silica and native silicon oxide substrates were examined. Figure 6 shows AFM images of 25.4 and 18.0 Å thickness films (films A and B, respectively) on native silicon oxide surfaces along with the corresponding reflection IR spectra. The spectra of the films respectively show C−H antisymmetric mode peaks at 2917 and 2930 cm^{-1}, an indication that the high-coverage film has highly conformationally ordered chains, whereas the low-coverage film has disordered, near liquid-like chains.

In an initial AFM scan of the thick film (A) with the tip placed under a high load (1500 nN), an 11 ± 1 Å deep indentation (pit) resulted. After a second scan inside the same region, the pit depth increased only slightly to 13 ± 1 Å, leaving a ∼12 ± 1 Å (25.4 Å − 13 Å) residual film in the scanned area. At this point, the tip became blunt from wear, thus preventing any further removal (shaving) of film material. With smaller loads (∼1000 nN), shallower pits resulted. Though the depth of such pits at this load increases with increasing number of scans, even after four scans at ∼1000 nN the observed depth was only ∼6 Å and did not increase significantly with additional scans. It is important to note that the raised height to the left and right of the shaved regions along the scanning direction in Figure 6 are imaging artifacts, not accumulation of debris, as evidenced by the observation that, when the imaging scan direction is rotated 90° to the original shaving direction such that no debris should be seen at the image scan range ends, the pattern remains the same (data not shown).

When the same measurements were performed using a fresh tip on the lower coverage film (B), after two scans at 1500 nN, the observed indentation depth was only ∼4 Å ± 1, leaving a ∼14 ± 1 Å (18.0 Å − 4 Å) residual film in the scan area. Increasing the load caused the tip to break without any shaving.

These results show that it is not possible, even at high tip loads, to completely remove the OTS molecules in either high- or low-coverage films down to the bare substrate. Rather, it appears that the combination of compressive and shear forces have a net effect of both removing some fraction of the original film and compressing the other fraction into a residual, dense, wear-resistant layer ∼12−14 Å thick. Leaving aside the mechanism for this behavior, we point out that strictly from the point of view of an analytical measurement we conclude that the starting film thickness (d_o) can be estimated from the relationship d_o(Å) ∼ 13 + d_P, where d_P is the depth of the etched pit after two scans with a tip loading of 1500 nN.[29] In a test of this relationship, another low-coverage film of 18.2 Å thickness was run with a resulting indentation of 5 ± 1 Å. Application of the equation gives a thickness of ∼18 Å, in excellent agreement with the actual film thickness value.

When identical experiments were performed on the fused silica substrates, similar results were obtained. In Figure 7, IR reflection spectra and AFM images of three OTS films with different coverages are shown. Since the silica substrates have a nearly identical refractive index at 633 nm to that of an OTS film, ellipsometric measurements were not able to provide film thicknesses. Film A is very low in coverage, as shown by the low contact angles and the appearance of the C−H antisymmetric stretching mode IR peak at 2923 cm^{-1}. When shaving was performed on this film, even at a relatively low tip load, the AFM tip consistently broke. This response indicates that the film was too thin to prevent the tip from making contact with the SiO_2 substrate and fracturing under the high loading. On the other hand, film B, with a relatively higher coverage than film A, as indicated by the higher contact angles and lower IR peak positions (see Figure 7), shows an observed 4 Å indent depth. Presuming that a uniform ∼13 Å residual film formed with the tip scans, we calculate a starting film thickness of 17 Å. This value seems quite reasonable, given the good agreement of the contact angles and IR spectra with the 18 Å film on native SiO_2. Finally, on the highest coverage film (film C), which shows contact angles and IR peak positions starting to approach the high-coverage films on the native oxide silicon substrates, the observed indent depth was ∼8 Å, giving a starting film thickness of 21 Å.

These results indicate that AFM shaving measurements can be a reliable tool for estimating the thickness of OTS films on hard substrates. Indentation depths of ∼10 Å indicate near complete monolayers with conformationally ordered, extended alkyl chains. In contrast, for very low coverage films, indentation measurements are not possible, due to tip penetration to the substrate. The reasons underlying the compression limit of ∼12−14 Å deserve further investigation, and here we only speculate on a few possible mechanisms. First of all, for a highly organized OTS film, the limiting density is near 5.42 chains/nm^2, with a thickness approaching 26.4 Å.[25] For our highest coverage film

(25) Xiao, X. D.; Liu, G. Y.; Charych, D. H.; Salmeron, M. *Langmuir* **1995**, *11*, 1600.
(26) Liu, G. Y.; Xu, S.; Qian, Y. *Acc. Chem. Res.* **2000**, *33*, 457.
(27) Bhushan, B.; Kulkarni, A. V.; Koinkar, V. N.; Boehm, M.; Odoni, L.; Martelet, C.; Belin, M. *Langmuir* **1995**, *11*, 3189.
(28) Garcia-Parajo, M.; Longo, C.; Servat, J.; Gorostiza, P.; Sanz, F. *Langmuir* **1997**, *13*, 2333.

(29) This relationship is based on shaving measurements performed on several different locations of the two films (films A and B) discussed in the text.

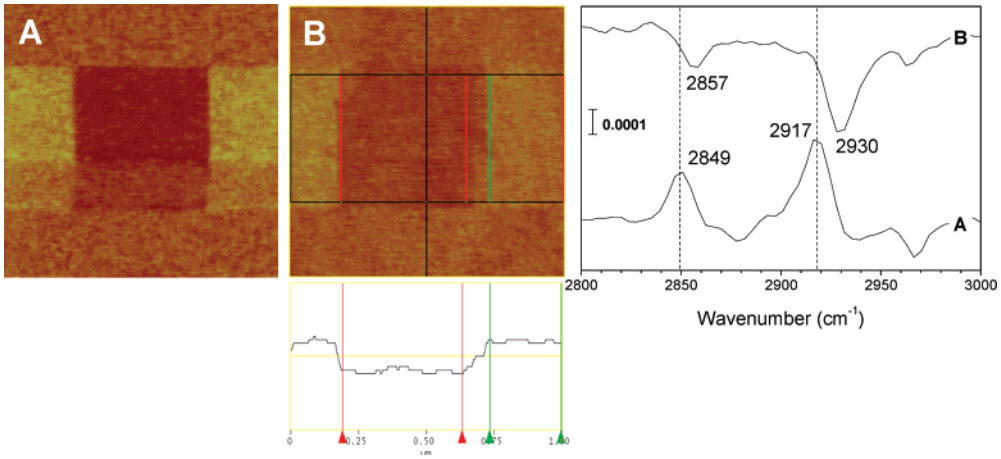

Figure 6. Contact-mode AFM images ($1 \times 1\ \mu m^2$, *z*-scale = 5 nm) of two OTS films on native oxide silicon surfaces with different coverages (left two panels) and the corresponding IR spectra (right panel). Film A has an ellipsometric thickness of 25.4 Å and advancing and receding contact angles of 42 ± 2° and 37 ± 2°, respectively. The depth of the indent formed after one scan at 1500 nN on this film is 11 Å. Film B has an ellipsometric thickness of 18.0 Å and advancing and receing contact angles of 25 ± 3° and 13 ± 3°, respectively. After two scans at 1500 nN, an indent with a depth of 4 Å formed on this film (second image). Average indent depths were determined by the "stepheight" module of the NanoScope software, and a representative screen shot for film B (full scale height variation of ±1 nm) is shown below the image for B. Spectrum A was taken from a companion film with an ellipsometric thickness of 24.7 Å.

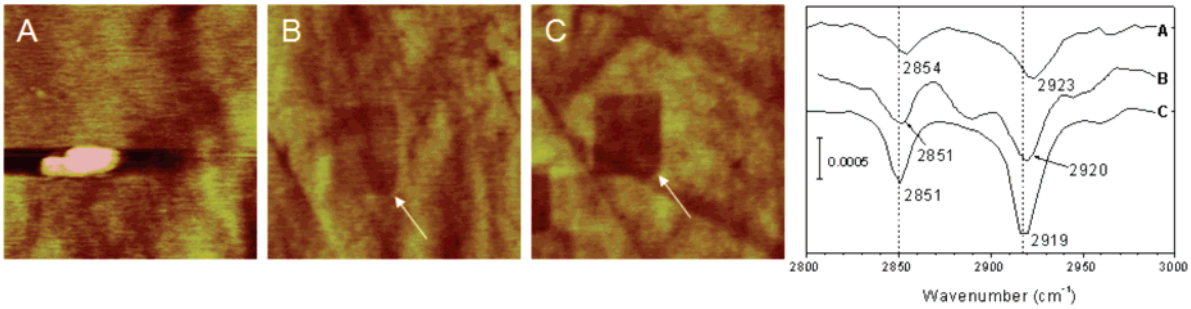

Figure 7. Contact mode AFM images ($1 \times 1\ \mu m^2$, *z*-scale = 5 nm) of three OTS films on fused silica surfaces with different coverages (left three panels) and the corresponding IR spectra (right panel). Film A has advancing and receding contact angles of 27 ± 4° and 13 ± 7°, respectively. After one scan at 1100 nN on this film, the AFM tip breaks (leftmost image). Film B has advancing and receding contact angles of 36 ± 2° and 32 ± 2°, respectively. After three scans at 2100 nN on this film, an indent with a depth of 4 Å forms (second image from the left). Film C has advancing and receding contact angles of 41 ± 2° and 36 ± 3°, respectively. After three scans at 2100 nN on this film an indent with a depth of 8 Å forms (third image).

of 25.4 Å (data shown in Figure 6), the molecular packing density should be close to 5.2 chains/nm^2. This value is very close to the ideal, so there is not enough free volume in the film to allow more than a small fractional compression without removing material by either dislodging of integral molecules or bond scission. Dislodging of individual molecules seems unlikely, since this would likely require attachment of a very unreactive terminal $-CH_3$ or a chain $-CH_2-$ moiety to the silicon oxide layer on the tip followed by extraction from the surface as the tip moves. Further, since the alkylsiloxane adsorbate species are extensively bonded to substrate silanol and/or cross-linked to neighboring alkylsiloxane headgroup −OH moieties, integral molecule removal would require selective breaking of either a Si−O−Si headgroup−substrate or headgroup−headgroup cross-link, while leaving all other bonds (Si−C, C−C, and C−H) intact. In fact, even without the existence of head group−substrate bonding (e.g., OTS on mica), it was shown that removal of a cross-linked network of OTS molecules from the surface needs higher energy than that of a non-cross-linked film (i.e alkanethiols on gold).[25,30] In addition, since adsorbate Si−O−Si bond formation (either to the surface or to the neighboring molecules) occurs rather late during the film growth,[19,24] our films, with long silanization exposures (∼18 h), should have a high fraction of covalently bonded headgroups. Besides, the AFM shaving experiments were performed between hours to days after the silanization, thus leaving ample time for completion of the cross-linking. As a further check of the effect of cross-linking, film A (on native oxide) was heated at 120 °C for 15 min, which should increase cross-linking even further. After cooling, indentation (one scan, 1500 nN) in a previously unscanned area of the film, however, resulted in an ∼8 Å pit depth (AFM images not shown), in contrast to the deeper indentation value of ∼11 Å obtained before heating. While this result suggests that some small fraction of the film removal could be due to release of whole molecules, overall the most likely process would seem to be bond scission and molecular fragmentation. However, if the latter mechanism is actually the dominating one, then this suggests, based on the ∼13 Å "compression" limit, that bond scission or molecular fragmentation can occur only to a certain degree. The reason to this may be that, as the thickness of the organic layer between the AFM tip and the SiO_2 substrate decreases, the remaining organic layer gets mechanically harder, which then causes the tip to fracture without any further compression or

(30) Berger, R.; Cheng, Y.; Forch, R.; Gotsmann, B.; Gutmann, J. S.; Pakula, T.; Rietzler, U.;Schartl, W.; Schmidt, M.; Strack, A.; Windeln, J.; Butt H.-J. *Langmuir* **2007**, *23*, 3150.

Table 1. Water Contact Angles Measured in 50 μm Capillaries as a Function of CO_2 Pressure and Reaction Time[a]

sample	CO_2 pressure, MPa	reaction time, min	adv angle, ±4° (speed, μm/s)	rec angle, ±4° (speed, μm/s)
I	15.4	360	83 (1.6)	74 (1.6)
II	14.0	240	84 (2.8)	74 (2.6)
III	13.6	540	91 (1.1)	90 (1.1)
IV	13.6	360	93 (1.5)	87 (1.5)
V	13.6	5	59 (2.2)	44 (2.2)
VI	13.4	60	84 (4.2)	78 (4.2)
VII	13.4	15	85 (3.6)	75 (3.6)
VIII	12.1	240	95 (1.6)	82 (1.0)
IX	8.6	120	97 (2.8)	90 (2.9)
X	8.6	2.5	90 (1.5)	77 (1.5)
XI	10.3	180	98 (2.1)	90 (2.1)
room temperature water flushed clean capillary			41	37
hot water flushed clean capillary			36	35

[a] The flow rates of probe fluid (water) during the measurements are also given in the last two columns in parentheses. The capillaries were pretreated with room-temperature water for films I−X and were pretreated with hot water for film XI. Since the contact angles showed variations along the length of the capillaries, the best available contact angles (highest values with lowest available hysteresis) at the indicated speeds are reported for each set of deposition parameters.

molecular fragmentation. In fact, such a hardening mechanism is observed on amorphous OTS films on native oxide silicon surfaces.[28]

3.2. Film Formation in the Single Capillaries and Microstructured Optical Fiber Capillary Arrays. *3.2.1. Contact Angle Measurements.* For the capillary wetting measurements, water was used as a contact angle liquid instead of hexadecane, since a significant number of films formed during the film process development were of low coverage, which typically on planar SiO_2 surfaces would be close to wetting (∼10°) for hexadecane, where contact angles cannot be accurately measured. In contrast, water always shows quite large contact angles, which allows a wide range in the wetting vs film coverage correlations. The advancing water contact angles on flat surfaces (of dense OTS monolayers composed of *all-trans*-alkyl chains arranged perpendicular to the surface) have actually been reported to be as high as 115°.[24] The advancing and receding angles, measured using microscope imaging of trapped air bubbles, for OTS-coated capillaries as a function of the silanization time and the CO_2 pressure are summarized in Table 1, along with data for the clean capillaries.[31] First, we note that the clean capillary control data (Figure 8) show that even with hot water treatment the silica surfaces do not become completely wettable (contact angles of ∼15°−35°) and thus exhibit only a limited concentration of surface silanols, as compared to the planar surfaces, where complete wetting can be observed. For the OTS films, two trends are apparent: (1) similar to what is observed on flat surfaces, there is a rapid increase in the film coverage very early during film growth and (2) as the amount of CO_2 introduced in the reaction vessel increases, the time needed for completion of the film also increases. As an example of the second trend, when the CO_2 pressure was 8.6 MPa, very high contact angles were observed, even only after 2.5 min of deposition. At 15.4 MPa, however, even after ∼6 h of deposition, the measured contact angles were smaller. We speculate that this behavior is due to the higher CO_2 density increasing the transport of the OTS molecules along the capillary, which results in a reduced interaction time of the molecules with the capillary walls and a corresponding reduction in silanization efficiency. In the light of these data, we picked 8.6−10.3 MPa and 2−3 h as the optimum CO_2 pressure and reaction time. In no case, however, were we able to measure advancing contact angles higher than 100°.

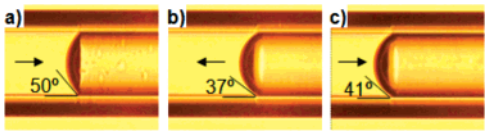

Figure 8. Images of a water meniscus moving inside a room temperature water flushed 50 μm capillary. The lighter colored regions at the left side of each image are water. Arrows show the direction of motion. See ref 25 for discussion.

Attempts to drive the OTS coverages higher to achieve higher contact angles only resulted in films with average thicknesses in excess of one monolayer and for which AFM (film XI in Table 1) and optical microscope images (Film IV in Table 1) showed the presence of clusters. These clusters were ascribed to polymerized OTS clusters, as shown by both micro-Raman and IR microscope analyses (data not shown). The limiting contact angle for the single layer films appears to be near 100° with the value perhaps set more by the capillary effects on the measurement than by the film coverage.

More information can be extracted from the contact angle results by examining the hysteresis values, their variation as a function of the position along the length of the capillary, and the speed of the meniscus (contact line). As seen in Table 1, for some films the hysteresis was minimal, whereas for others it was as high as 15° (e.g., compare film V to film III). The film quality and the coverage have an effect on these values, but these two effects alone may not be enough to explain the data. The data show a trend of decreasing hysteresis with increasing deposition time (films V and VI, films IX and X); however, the same cannot be said for the film quality (uniformity). For example, two films, one having high concentration of polymerized OTS clusters visible by AFM (film XI) and another with no such clusters (film IX), have about the same level of hysteresis. Last, while for some films the variation in the contact angles as a function of the meniscus speed and the location along the capillary in a few centimeters long region were minimal (a few degrees), for some others considerable variations were observed. For example, for film III, at a certain location along the capillary the contact angles were high and did not change with increasing meniscus speed (adv 100°, rec 84°); however, about 0.5 mm from this region contact angles were much smaller and showed considerable variation as a function of the meniscus speed (adv 101° and rec 66° at 16 μm/s, adv 100° and rec 72° at 8 μm/s). Interestingly, even when receding angles change as a function of position and/or speed, the change in the advancing angles was minimal. These variations in the contact angles indicate that film variations along the capillary may either be caused by the pressure gradients that form in the capillaries during the deposition or the inefficient rinsing of the films after the deposition. Overall, the contact angle data reported in Table 1 give a good qualitative characterization of the films, since a partial monolayer (film V) can be

(31) The receding contact angle for clean capillaries flushed with room temperature water is 37° (see Figure 8b) and remains fairly constant for a variety of treatment conditions. In contrast, the advancing angle varies considerably with the treatment. When the contact line is situated with the vapor side in a region never prewet by liquid, the advancing angle was observed to be as high as 50° (see Figure 8a), an indication of a very low surface silanol coverage. But when the vapor side is in a previously wetted region, where surface silanol coverage could increase due to hydrolysis, the advancing angle approached the value of the receding angle (see Figure 8c). In a hot water flushed clean capillary, on the other hand, the advancing angle was equal to the receding angle (∼36°), regardless of the history of the vapor phase capillary section at which the measurements were made. In this case, the higher temperature appears to cause rapid hydrolysis and water adsorption ahead of the contact line, which results in equal advancing and receding angles. These results show the importance of the presence or absence of a leading edge water film at the silica surface contiguous with the contact line. (See Kalliadasis S.; Chang H. C. *Phys. Fluids* **1994**, 6, 12.)

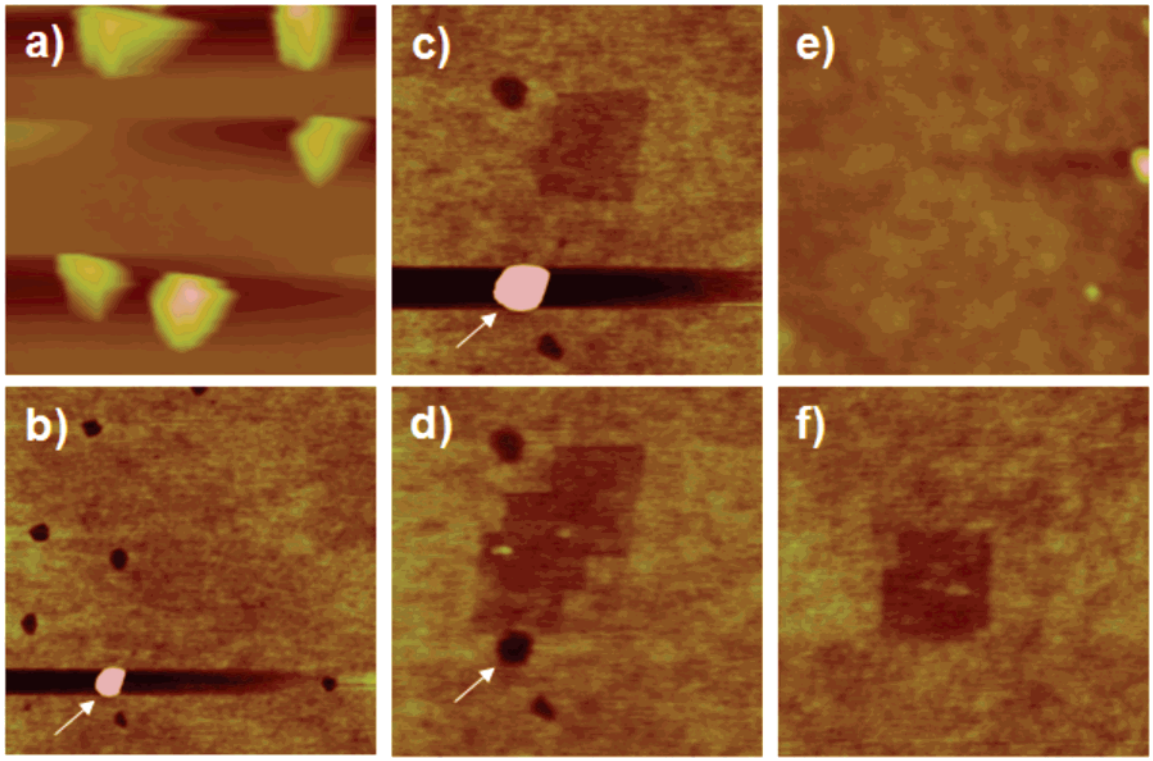

Figure 9. AFM images of films XI (a−d) and IX (e, f), whose wetting properties are reported in Table 1. (a) Tapping-mode image of film XI. Image size is 1 × 1 μm^2, *z*-scale is 100 nm. (b) Contact-mode image of the same film. The arrow shows the only OTS cluster that could not be removed by the AFM tip. Image size is 2 × 2 μm^2, *z*-scale is 5 nm (c) Contact mode image of the section shown in part b, after two scans at 1150 nN. The arrow points to the same OTS cluster shown in part b. Indent depth = 5 Å, image size is 1 × 1 μm^2, *z*-scale is 5 nm. (d) Contact-mode image of the section shown in part c after three more scans at 1500 nN. The resulting pattern is due to the drift of the tip during the scan. The arrow shows the original position of the OTS cluster that can be seen in parts b and c. Indent depth = 7 Å, image size is 1 × 1 μm^2, *z*-scale is 5 nm. (e) Tapping-mode image film IX. Image size is 1 × 1 μm^2, *z*-scale is 10 nm. (f) Contact-mode image of the same film after one scan at 1150 nN and one scan at 1500 nN. Indent depth = 8 Å, image size is 1 × 1 μm^2, *z*-scale is 5 nm.

distinguished from an intermediate (film I) or a high coverage (film IX) film. Further studies of the contact angles are needed to sort out the role of capillary effects from the film coverage/quality and the meniscus speed.

To facilitate deposition in microstructured optical fibers with smaller inner dimensions, a completely ncCO$_2$ process was devised using wet ncCO$_2$ to increase the surface silanol concentration and a chloroform/ncCO$_2$ postdeposition rinse. Advancing (99°) and receding (89°) contact angles measured on 50 μm single capillary microstructured optical fibers using this process are similar to those determined for experiments for which the capillaries were flushed with liquid water and liquid chloroform. Contact angle results for principally ncCO$_2$ deposition demonstrate that high-coverage OTS films can be deposited in microstructured optical fibers using an entirely supercritical or near critical fluid process.

3.2.2. Atomic Force Microscopy. A series of AFM images (Figure 9) for two films (IX and XI in Table 1), formed in 50 μm capillaries, were obtained from broken sections of the capillaries. Tapping mode images of film XI, which was grown in a hot-water-flushed capillary, shows formation of OTS clusters, presumably arising from the high concentration of surface water in the hot water pretreatment. When contact mode imaging was performed on the same film at a 50 nN tip loading, all but one of the OTS clusters were observed to be wiped away by the AFM tip (Figure 9b). Subsequent line scans at the same force loading along the resulting pits showed depths ranging from 18 to 28 Å, values in the range of the thicknesses of OTS monolayers from moderate to high coverages. This result suggests that the OTS clusters form early in the silanization and prevent formation of an OTS monolayer on the underlying silica substrate.

When a 250 nm^2 area, at the center of same region, was scanned twice at ∼1100 nN tip load, an indentation with an average depth of 5 Å formed (Figure 9c). We then tried to scan the same 250 nm^2 area, at ∼1500 nN tip load, to find out if the indent depth would increase further. However, during this process the tip has drifted toward the OTS cluster located at the lower part of the imaged region (indicated with arrows in Figure 9b,c) and eventually wiped away this cluster, producing a pit adjacent to the shaved area. As can be seen in Figure 9d, the shaved area and the adjacent newly formed pit have different heights. The average depth of the shaved region is 7 Å, whereas the average depth of the pit left behind by the removal of the OTS cluster (indicated by an arrow in Figure 9d) is 25 Å. This observation actually confirms our suggestion that even a complete monolayer of OTS can only be compressed by at most about 11 Å, as evidenced by the height difference of the shaved region and the adjacent pit.

When similar measurements were performed on the film grown in room temperature water flushed capillary (film IX), it was observed that the number and size of the polymerized OTS clusters were much less (Figure 9e). However, the depth of the shaved region was still high, and after one scan at 1100 nN followed by a second scan at 1500 nN, it was observed to be about 8 Å (Figure 9f). When combined with the contact angle data, these results suggest that, even though hot water treatment produces higher water concentration at the surface, room temperature water treatment is enough for preparation of a complete monolayer, without extensive formation of polymerized OTS clusters.

3.2.3. UV/Ozone Treatment. Finally, we investigated methods for selective film removal in specific regions inside of the capillaries to evaluate possibilities for lithographic patterning,

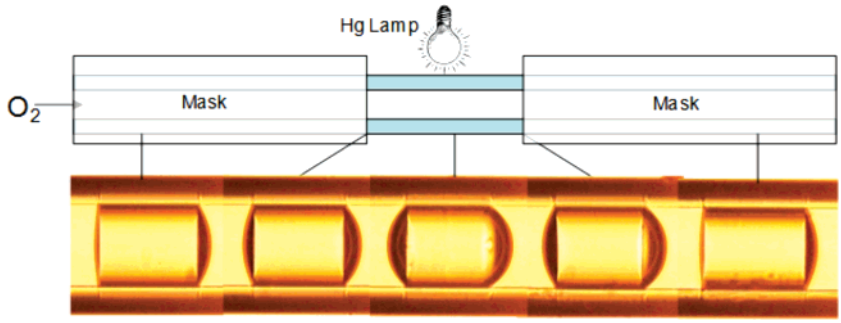

Figure 10. Images of an air bubble moving (to the right) inside an OTS-coated 50 μm capillary, after UV/ozone treatment.

for example, to form functional molecule or nanoparticles patterns.[2] This capability potentially allows for nanofabrication in all three dimensions: the pattern in two dimensions is set by the microstructured optical fiber template, while control in the third dimensions is provide by the ability to pattern along the length of the fiber. An OTS-coated capillary, which had advancing and receding contact angles of 84° and 66°, respectively, was flushed with O_2, while a 1 cm section of the capillary was exposed to UV light by means of a mask (pictured schematically in Figure 10). After 30 min of UV exposure, the contact angles at the UV-exposed section of the capillary were 52° (adv) and 36° (rec), equal within experimental error to the values measured in the room temperature water flushed clean capillary, whereas, in contrast, no significant change was observed in the contact angles of the nonexposed sections.

4. Conclusions and Future Work

We have demonstrated that well-organized, densely packed OTS films can be prepared in microstructured optical fiber silica capillaries by using $ncCO_2$ or $scCO_2$ as the reaction solvent. Comparison of shaving results in microcapillaries with those performed on complete monolayers on flat surfaces composed of highly trans extended alkyl chains as indicated by the reflection IR spectra suggests that the films in the capillaries exhibit alkyl chains with a high degree of conformational ordering and dense packing. Wetting measurements proved to be very useful for determining the film coverage and homogeneity in the capillaries. Nevertheless, more detailed and systematic wetting measurements are needed in order to understand the underlying mechanisms that control the wetting properties in the capillaries and to distinguish effects of film coverage and quality from the capillary effects. Using the same film preparation methodology, but using silane molecules with different end groups, the capillary walls can be functionalized controllably. We compared processing with liquid water for surface hydroxylation and liquid chloroform for removing excess OTS with the use of water dissolved in $ncCO_2$ and chloroform dissolved in $ncCO_2$ for the same purposes. Similar contact angles were achieved in both cases, indicating that processing solely with high-pressure CO_2 is possible, which will be useful for silanization of capillaries of nanoscale dimensions. The films were characterized by wetting and AFM shaving measurements. This capability, together with the ability to generate interior patterns, could have potential applications in areas such as chromatography and chem/bio sensors.

Acknowledgment. J.V.B. and D.L.A. acknowledge support from the Penn State Materials Research Institute, the Office of Naval Research, and the US Department of Agriculture. P.J.A.S. acknowledges support from the UK Engineering and Physical Sciences Research Council.

LA703155Z